© 2008 International Society of Nephrology

Aristolochic acid induces proximal tubule apoptosis and epithelial to mesenchymal transformation

AA Pozdzik[1], IJ Salmon[2], FD Debelle[1,3], C Decaestecker[4], C Van den Branden[5], D Verbeelen[6], MM Deschodt-Lanckman[1], J-L Vanherweghem[3] and JL Nortier[1,3]

[1]Experimental Nephrology Unit, Faculty of Medicine, Erasme Hospital, Université Libre de Bruxelles (ULB), Brussels, Belgium; [2]Department of Pathology, Erasme Hospital, Université Libre de Bruxelles (ULB), Brussels, Belgium; [3]Department of Nephrology, Erasme Hospital, Université Libre de Bruxelles (ULB), Brussels, Belgium; [4]Laboratory of Toxicology, Institute of Pharmacy, Université Libre de Bruxelles (ULB), Brussels, Belgium; [5]Menselijke Anatomie, Vrije Universiteit Brussel, Brussels, Belgium and [6]Department of Nephrology, Vrije Universiteit Brussel, Brussels, Belgium

Aristolochic acid contamination in herbal remedies leads to interstitial fibrosis, tubular atrophy, and renal failure in humans. To study the cellular mechanisms contributing to the pathophysiology of this renal disease, we studied Wistar rats treated with aristolochic acid and measured tubular and interstitial cell proliferation, epithelial/mesenchymal cell marker expression, tubular membrane integrity, myofibroblast accumulation, oxidative stress, mitochondrial damage, tubular apoptosis, and fibrosis. Oxidative stress, a loss of cadherin concomitant with vimentin expression, basement membrane denudation with active caspase-3 expression, and mitochondrial injury within tubular cells were evident within 5 days of administration of the toxin. During the chronic phase, interstitial mesenchymal cells accumulated in areas of collagen deposits. Impaired regeneration and apoptosis of proximal tubular cells resulted in tubule atrophy with a near absence of dedifferentiated cell transmembrane migration. We suggest that resident fibroblast activation plays a critical role in the process of renal fibrosis during aristolochic acid toxicity.

Correspondence: JL Nortier, Department of Nephrology, Erasme Hospital, Université Libre de Bruxelles (ULB), Route de Lennik 808, B-1070 Brussels, Belgium. E-mail: jnortier@ulb.ac.be

The respective role of epithelial to mesenchymal transition (EMT) of tubular epithelial cells and inflammatory cells in the progression of tubulointerstitial (TI) lesions—from tubular necrosis to interstitial fibrosis—remains a matter of debate.[1,2] We decided thus to investigate some aspects of those processes in the rat model of aristolochic acid (AA) nephrotoxicity. Aristolochic acid nephropathy (AAN) is a TI nephritis of toxic origin rapidly progressing to fibrosis reported in individuals after the intake of AA contained in some herbal remedies.[3] Renal function deteriorated rapidly, leading to end-stage renal failure in several months.[3] The progression of AAN was characterized by variable intensity of lymphocyte infiltration, prominent tubular atrophy, and TI fibrosis with microscopically intact glomeruli.[4] Prior exposure to AA resulted in specific AA–DNA adducts formation in kidney tissue samples, detectable even years after AA intoxication.[5,6]

Human AAN was reproduced in rabbit and rodents.[7,8] In Wistar rats, AA intoxication resulted in tubular atrophy and interstitial fibrosis leading to renal failure after 35 days.[8] An early tubular proteinuria was related to a defect of megalin-mediated endocytosis of albumin by the proximal tubular epithelial cells (PTECs), confirming previous in vitro observations.[9,10] After approximately 20 days of AA injection, a transient decrease in proximal tubule enzymuria was observed,[9] reflecting an attempt of PTEC regeneration. Physiologically, renal repair after acute injury is conditioned by regeneration and proliferation of surviving epithelial cells.[11,12] As in vivo and in vitro studies confirmed the formation of specific AA–DNA adducts in renal epithelial cells,[5,6,9,10] these adducts could interfere with PTEC proliferation capacity, negatively influencing regeneration. However, the implication of apoptosis has been demonstrated in models of chronic kidney disease and should also be considered as a possible mechanism of tubular epithelial cell deletion.[13]

We thus hypothesized that AA sustained intoxication results in altered PTEC regeneration and apoptosis leading to subsequent irreversible proximal tubular atrophy. Moreover, as atrophic tubules were surrounded by interstitial fibrosis,

we investigated the presence of EMT as a potential mechanism of renal scarring. The defining steps of EMT were adapted from Yang and Liu[14] as follows: (1) loss of epithelial cell adhesion, (2) vimentin and alpha smooth muscle actin (α-SMA) expression, (3) tubular basement membrane disruption, and (4) migration of dedifferentiated cells across this disrupted membrane. Finally, we addressed the association between changes in oxidative stress parameters and PTEC apoptosis with the development of morphological changes (fibrosis and tubular atrophy).

This study demonstrated that AA tubulotoxicity resulted in defective activation of antioxidative enzymes and mitochondrial damage. The progressive tubular atrophy was related to impaired regeneration and apoptosis of PTEC. Transmembrane migration of PTEC displaying signs of EMT was rarely observed. The accumulation of vimentin and of α-SMA-positive cells in the interstitial areas expressing transforming growth factor-β (TGF-β) suggested an increase in resident peritubular fibroblasts and their activation into myofibroblasts. Therefore, the activated resident fibroblasts could be considered as the main source of collagen deposition during experimental AAN.

RESULTS
TI injury, renal structural and functional markers
TI injury. In the process of experimental AAN, we have arbitrarily distinguished two phases: an acute phase from day 1 to day 5 and a chronic phase from day 7 to day 35.

Glomeruli were intact in both rat groups. In AA rats, during the acute phase, signs of oncosis (decreased cytoplasm eosinophilia reflecting PTEC swelling) and patchy PTEC necrosis were limited to the outer stripe of outer medulla (OSOM) (segment S3) (Figure 1a–c). During the chronic phase, in these areas, tubules became progressively atrophic and exhibited typical basement membrane thickening (Figure 1d–f). As compared to controls, the total tissue kidney surface from AA rats at day 35 was significantly reduced ((median value (min–max) in mm^2 per field): 0.034 (0.031–0.037) vs 0.041 (0.037–0.043), $P < 0.05$).

The score of TI injury obtained in AA rats revealed a peak of tubular necrosis at days 4 and 5 (Figure 1g), followed by progressive tubular atrophy and interstitial fibrosis (Figure 1h and i, respectively). A marked lymphocytic infiltration was also present (Figure 1j).

Renal structural and functional markers. In AA rats, as compared to controls, a transient increase in PTEC brush-border DPPIV (dipeptidyl peptidase IV) enzymuria (median value (min–max) in μmol AMC (7-amido-4-methyl-coumarin) product per g creatinine (Cr)) was measured at day 4 (687 (607–765) vs 563 (415–744), $P < 0.05$) followed by a significant decrease as early as day 7, which persisted until day 35 (day 7: 185 (147–313) vs 328 (282–410), $P < 0.01$; day 10: 81 (48–118) vs 133 (96–171), $P < 0.05$; day 14: 182 (147–275) vs 387 (276–497), $P < 0.01$; day 18: 216 (173–271) vs 356 (268–512), $P < 0.01$; day 35: 280 (157–369) vs 527 (374–777), $P < 0.01$).

A significant increase in plasma Cr (median value (min–max) in mg per 100 ml) was observed from day 3 (0.336 (0.265–0.05) vs 0.222 (0.186–0.26), $P < 0.01$) to day 35 (0.345 (0.25–0.5) vs 0.245 (0.2–0.3), $P < 0.05$).

Interstitial inflammation and urinary excretion of monocyte chemoattractant protein-1
Contrasting with controls, the renal interstitium from AA rats was abundantly infiltrated with monocytes/macrophages and CD8 + lymphocytes from day 3 to day 35. These inflammatory cells accumulated around damaged PTECs from the OSOM (Figure 2a–c and d–f), where typical signs of CD8 + tubulitis, reflecting T-cell cytotoxicity, were evident (Figure 2g and h).

No statistically significant difference in the urinary excretion of monocyte chemoattractant protein-1 (MCP-1) was observed between AA rats and controls during the acute phase. On the contrary, urinary levels of MCP-1 were significantly increased from day 7 to day 35 in AA rats (Figure 2i).

Proliferation of tubular cells and DNA damage repair
In AA rats, Ki-67 + cells were observed from day 2 to day 35 (Figure 3a–c). During the acute phase, most of these cells were identified as PTECs from the S3 segment (neutral endopeptidase (NEP)/Ki-67 coexpression) (Figure 3d and e). The onset of tubular proliferation occurring at day 2 was concomitant with acute tubular necrosis (Figure 3f). During the chronic phase, the scores of Ki-67 + PTEC and of tubular atrophy correlated negatively ($n = 60$, $r = -0.758$, $P < 0.0001$). The amount of Ki-67 + interstitial cells reflected a sustained proliferation of infiltrating and/or resident cells from day 3 to day 35 (Figure 3g).

As of day 1, typical proliferating cell nuclear antigen positive (PCNA +) tubular and interstitial cell clusters were seen in the corticomedullary junction (Figure 4a and b). At day 35, PCNA labeling in atrophic tubules contrasted with strong PCNA expression in interstitial cells (Figure 4c). In the papilla, proliferating tubular cells were present only during the acute phase (Figure 4d–f) and were confined to the medullary ascending thick limb (PCNA + /cytokeratin 18−) and to the collecting ducts (PCNA + /cytokeratin 18 +) (Figure 4g). As compared to controls, the amount of PCNA + PTECs was higher in AA rats at all time points (Figure 4h). No correlation was found between the amount of Ki-67 + and PCNA + PTECs ($n = 60$, $r = 0.227$, $P = 0.084$).

PTEC dedifferentiation, tubular basement membrane denudation, and interstitial fibrosis
The percentage of NEP + PTECs significantly decreased throughout the chronic phase (Figure 5a). As soon as day 3, mature PTECs expressed *de novo* vimentin (mesenchymal cell marker). These dedifferentiated cells progressively accumulated within damaged nephrons, trapped by interstitial inflammation (Figure 5b–d). At day 35, atrophic tubules were colonized exclusively by vimentin + /NEP− cells
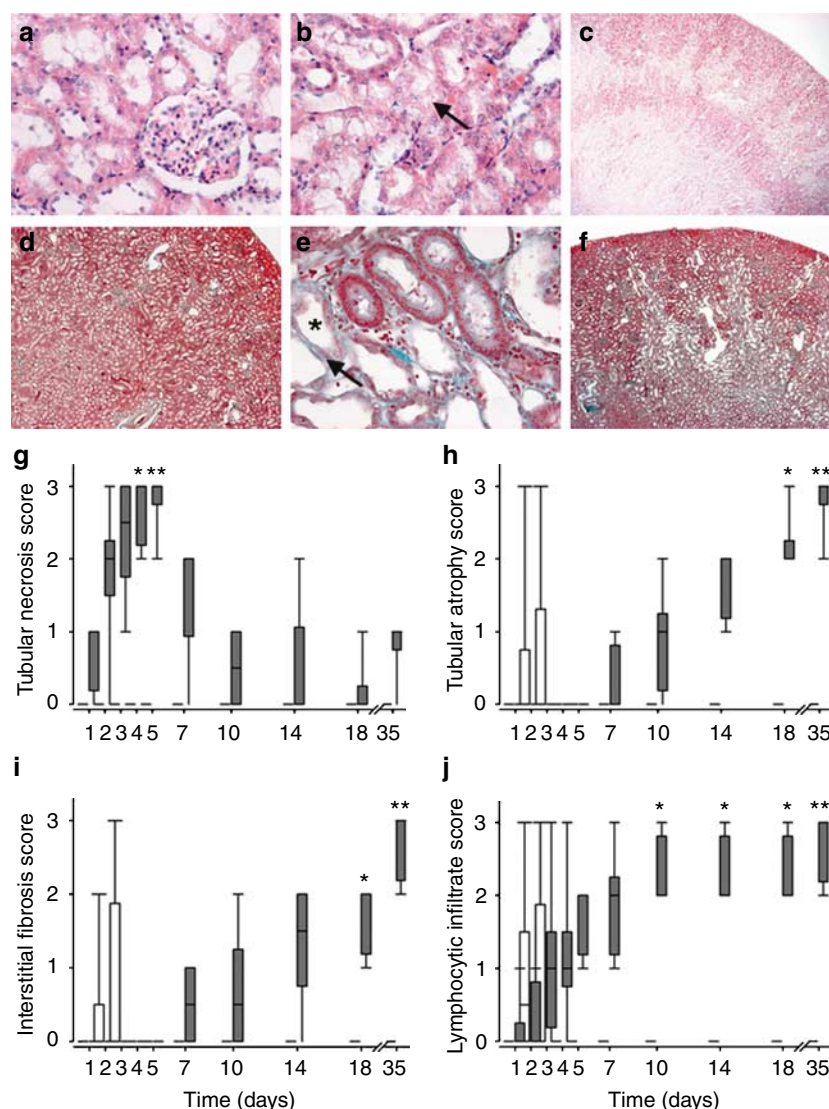
Figure 1 | Representative photomicrographs of kidney sections stained by hematoxylin/eosin and Goldner's trichrome. Time course of semiquantitative scores of TI injury. (**a** and **d**, day 35) Control rats exhibited intact renal parenchyma. (**b**, day 1) AA-induced PTEC oncosis demonstrated by organelle swelling (arrow) and (**c**, day 4) marked decrease in eosinophilia of PTEC from the outer medulla, including medullary rays. (**e** and **f**, day 35) Tubular degenerative changes, including PTEC atrophy (star) with thickening of the basement membrane (arrow). Typical areas of interstitial fibrosis extending along the medullary rays up to the subcapsular area observed in AA rats. Original magnifications: (**a**, **b**, and **e**) ×400; (**c**, **d**, and **f**) ×40. (**g–j**) As most data from controls (white boxes) at the majority of time points are close to zero, they are represented by horizontal lines. (**g**) Transient increase in the score of tubular necrosis from day 2 to day 5 in AA rats (gray boxes) was followed 2 weeks later by a progressive increase in the scores of (**h**) tubular atrophy and (**i**) interstitial fibrosis. (**j**) A significant increase in the lymphocytic infiltrate score persisted throughout the chronic phase. Data are median values together with the interquartile ranges and the min–max values; $*P < 0.05$, $**P < 0.01$ vs day 1.

(Figure 5e). Vimentin/Ki-67 coexpression confirmed their ability to proliferate (Figure 5f).

As early as day 3, NEP+ PTECs lost N-cadherin expression (as well as E-cadherin; data not shown). The disappearance of epithelial cell–cell adherent junctions was actually limited to the S3 segment of proximal tubules (Figure 6a–c). During the acute phase, marked early focal tubular basement membrane denudations were confirmed by ultrastructural analysis (electronic microscopy) (Figure 6d–h). Detached PTECs were found in the tubular lumen. The evidence of detached cell migration into the interstitium was almost absent.

Intense TGF-β expression by PTECs and adjacent interstitial cells was detected early (day 3) and persisted until day 35 (Figure 6i–k). From day 7 until day 35, S100A4+ interstitial mononuclear cells accumulated around injured PTECs from the S3 segment, which later became areas of interstitial scarring (data not shown). Acquisition of the myofibroblast phenotype (α-SMA expression) by tubular and interstitial cell clusters was seen during the chronic phase (Figure 7a–c). Sirius red staining revealed the tubular basement membrane anomalies at days 10 and 35 (Figure 7d–f). At day 35, foci of TI fibrosis identified by the apposition of collagen
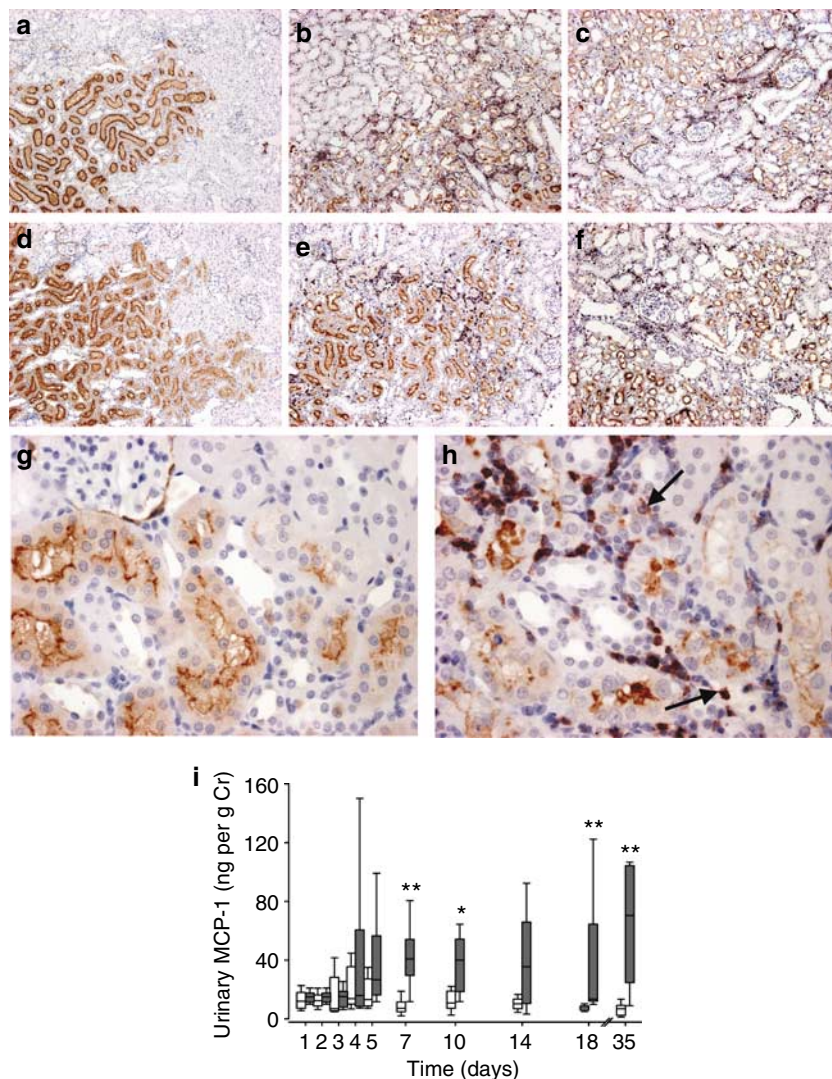
Figure 2 | Kidney NEP/ED1 (first row) and NEP/CD8 (second row) immunoperoxidase double stainings and MCP-1 urinary excretion rate during AAN. (**a** and **d**, day 10) Absence of ED1+ and CD8+ cell clusters in control rats. In AA rats, (**b** and **e**, day 10) ED1+ and (**c** and **f**, day 35) CD8+ cell clusters (colored in purple) were predominantly observed around injured tubules containing NEP-stained PTEC (colored in orange). After 10 days of injections, (**g**) absence of infiltrating CD8+ cells in controls and (**h**) intratubular cytotoxic CD8+ cells (tubulitis; arrow) in AA rats. Sections were counterstained with Mayer's hematoxylin. Original magnifications: (**a–f**) × 40; (**g** and **h**) × 400. (**i**) As compared to controls (white boxes), significant and sustained increase in MCP-1 urinary excretion rate measured from day 7 to day 35 in AA rats (gray boxes). Data are median values together with the interquartile ranges and the min–max values; *$P < 0.05$, **$P < 0.01$, ***$P < 0.005$ vs controls.

types I and III were typically located along the external part of the medullary rays (Figure 7g–l).

Oxidative stress, mitochondrial injury, and apoptosis

In the first 2 weeks, following a transient increase in the urinary excretion rate of nitric oxide metabolites (NOx) (median (min–max) μmol per mmol Cr), their excretion was decreased in AA rats as compared to controls (at day 1: 102.6 (83–109) vs 84.0 (42.1–90.4), $P < 0.05$; at day 14: 126 (107–155) vs 183 (148–218), $P < 0.005$). Renal cortex Mn-superoxide dismutase (SOD) activity did not significantly change throughout the protocol (Figure 8a). A sustained increase in glutathione peroxidase activity preceded a delayed decrease in Cu/Zn-SOD and catalase activities (Figure 8b–d).

At day 35, the cortical concentration of TBARSs (thiobarbituric acid reactive substances) (median (min–max) in pmol per mg protein) was 80.4 (78.5–84.0) in AA rats and 73.4 (66.2–84.6) in controls ($P = 0.054$).

Intoxication by AA induced changes in the immunostaining patterns of inducible nitric oxide synthase (iNOS) and cytochrome *c* in PTECs from the external parts of the medullary rays. After a transient enhancement of cytoplasmic iNOS staining (day 4), the expression dramatically decreased (Figure 9a–c). A strong, diffuse cytoplasmic cytochrome *c* staining reflecting their release from the internal mitochondrial membrane into the cytoplasm was detected in PTECs as soon as day 4 (Figure 9d and e). These modifications in cytochrome *c* expression persisted until day 35 (Figure 9f). From day 3 to
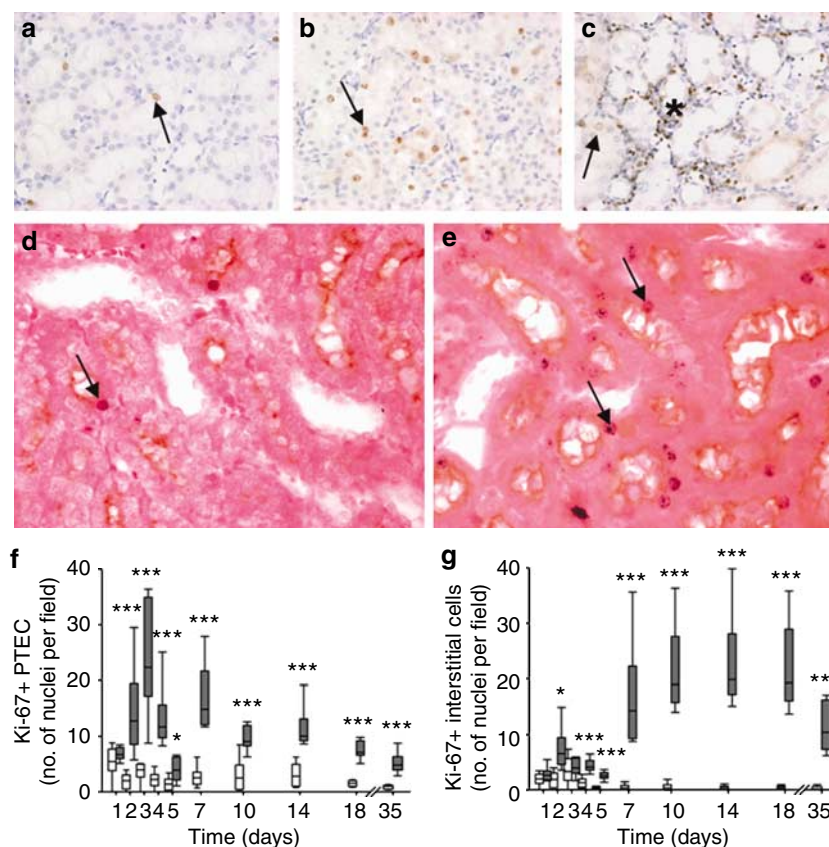
Figure 3 | Kidney Ki-67 and NEP/Ki-67 immunoperoxidase stainings. Time course of semiquantitative evaluation of Ki-67 expression by PTEC and interstitial cells. (**a**) Rare nuclear Ki-67 staining of PTEC in control kidneys (arrow). (**b**, day 3) Enhanced Ki-67 expression by PTEC in an AA rat (arrow). (**c**, day 35) Decreased Ki-67 expression by PTEC (arrow) contrasting with a dramatically increased Ki-67 expression by interstitial cells (star). (**d**) Rare NEP/Ki-67 coexpression in a control kidney (arrow). (**e**, day 4) Numerous NEP/Ki-67 double-stained PTECs in a representative AA rat (arrows). Sections were counterstained with (**a**–**c**) Mayer's hematoxylin or (**d** and **e**) eosin. Original magnification: ×400. (**f** and **g**) Sustained increase in Ki-67 labeling observed from day 2 to day 35 in tubular and interstitial compartments in AA rats (gray boxes), as compared to controls (white boxes). Data are median values together with the interquartile ranges and the min–max values; $*P<0.05$, $**P<0.01$, $***P<0.005$ vs controls.

day 35, PTECs (mainly from the S3 segment) and some distal tubular cells expressed active caspase-3 (Figure 9g–i).

DISCUSSION

The presently detailed time course of experimental AAN distinguished two interconnected phases: acute events occurring during the first phase (transient tubular necrosis) were complicated by the installation of chronic lesions seen during the second phase (tubular atrophy and TI fibrosis). The progressive peritubular accumulation of monocytes/macrophages and CD8+ T cells was the main process linking both phases. Indeed, the early transient AA-induced acute tubular necrosis might be considered as a crucial event triggering the chemoattraction of leukocytes.[15] In our study, the interstitial infiltration by inflammatory cells preceded increased urinary MCP-1 excretion. The persistence of interstitial inflammation during the chronic phase may be related to sustained urinary levels of this chemokine. According to the clinical and experimental data, TI infiltration by monocytes/macrophages and T lymphocytes is known to be associated with fibrogenesis.[16,17] Inflammatory

cells and injured PTEC-derived cytokines and chemokines (mainly MCP-1) by activation of neighboring fibroblasts contributes to excessive synthesis of the extracellular matrix and are important mediators of renal fibrosis.[16–18]

The S3 segment of proximal tubules, which is highly susceptible to hypoxia,[19] was the preferential target of AA. As intracellular activation/detoxification pathways are likely triggered by AA intoxication, the transient acute PTEC necrosis could reflect an imbalance between enhanced oxygen demand and delivery.[20] In addition to Ki-67, PCNA staining provided additional information regarding DNA damage. This polymerase cofactor is involved in DNA repair and stability of the DNA microsatellite region.[21] The disappearance of PCNA expression from PTEC might be considered as a defect of DNA repair in response to specific AA–DNA adducts formation ultimately leading to defective cell proliferation and the development of tubular atrophy. A similar interpretation was previously provided by experimental data obtained from the cisplatin model.[22] Moreover, cell cycle arrest of PTEC *in vitro* after AA exposure was recently reported.[23]
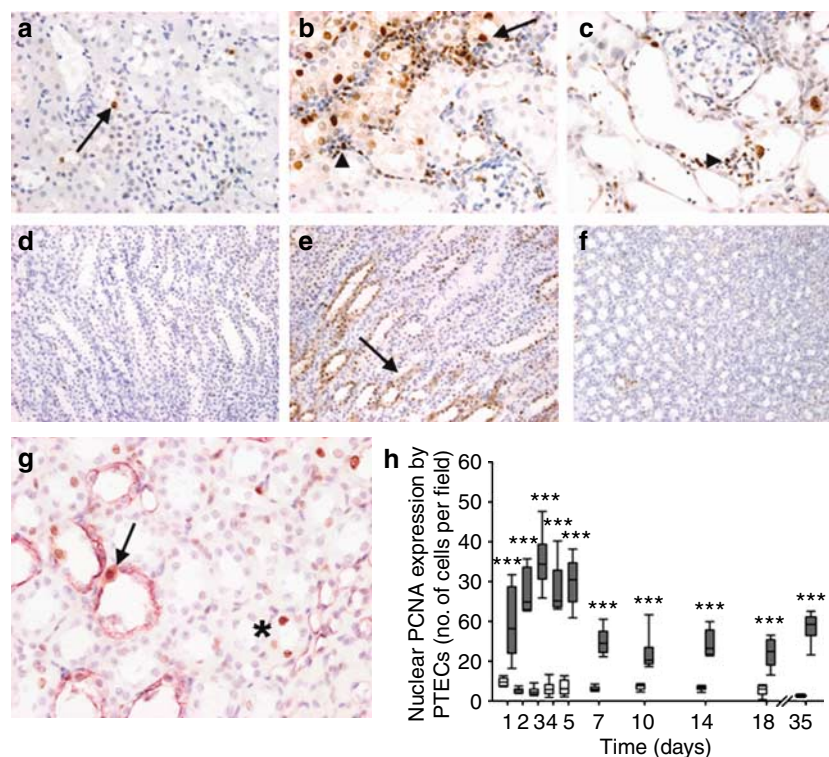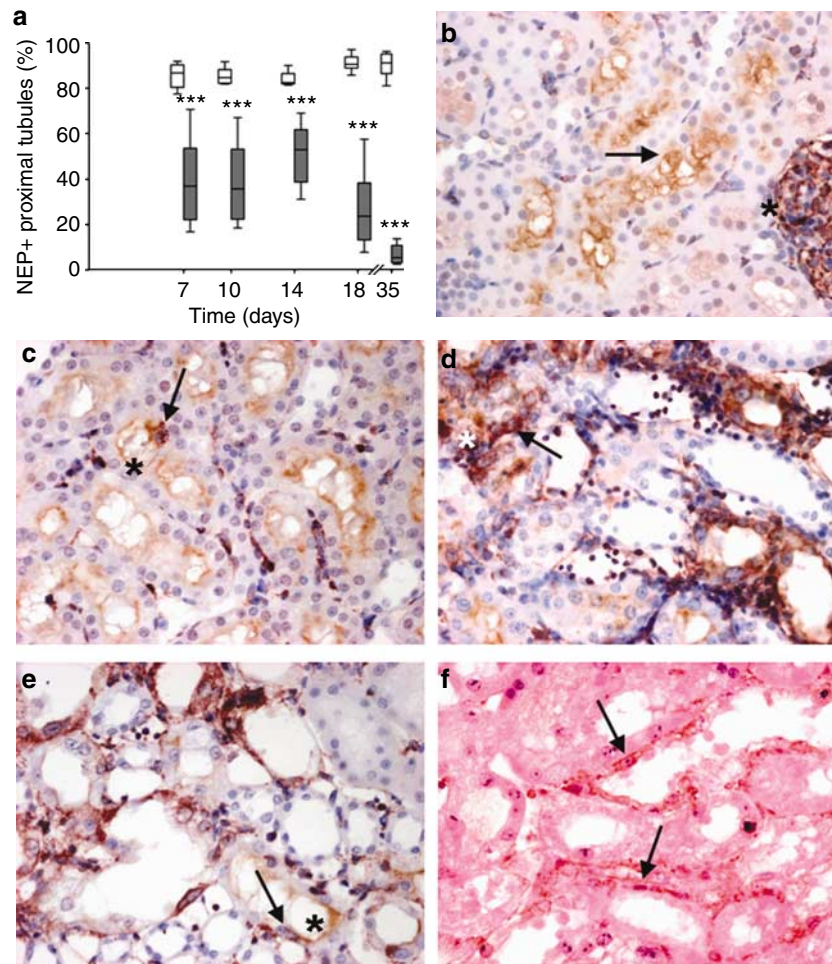
Figure 4 | PCNA immunoperoxidase staining (renal cortex and papilla) from representative control and AA rats. Time course of quantified PCNA expression in PTEC. *Renal cortex:* (**a**, day 1) sporadically PCNA-stained PTEC in controls (arrow), (**b**) PCNA staining in PTECs (arrow) and interstitial cells (arrowhead) at day 1 and (**c**) predominant PCNA expression by interstitial cells (arrowhead) at day 35 in AA rats. *Renal papilla*: in control, (**d**, day 4) absence of PCNA staining. In AA rats, (**e**, day 4) enhanced PCNA expression by papillary tubular cells (arrow) in conjunction with the disappearance of PCNA-stained papillary cells (**f**, day 35). (**g**, day 4) PCNA (brown)/cytokeratin 18 (red) double staining: PCNA expression by medullary thick ascending limb (cytokeratin 18 negative; star) and by collecting ducts (cytokeratin 18 positive; arrow). Sections were counterstained with Mayer's hematoxylin. Original magnifications: (**a–c** and **g**) ×400; (**d–f**) ×200. (**h**) Significant and persistent increase in PCNA expression by PTECs during both phases of AAN (gray boxes), as compared to controls (white boxes). Data are median values together with the interquartile ranges and the min–max values; *$P < 0.05$, **$P < 0.01$, ***$P < 0.005$ vs controls.

Acute AA tubulotoxicity resulted in early PTEC dedifferentiation reflected by the disappearance of the epithelial phenotype and acquisition of mesenchymal cell markers by some PTECs still expressing NEP. The regeneration of PTEC was confirmed by the proliferation of dedifferentiated cells (vimentin/Ki-67 coexpression), which should differentiate into mature epithelial cells under normal conditions.[24] In this model, regenerating cells might originate from injury-resistant resident progenitor-like tubular cells derived from the S3 segment, since PTEC proliferation was principally observed in the OSOM. Nevertheless, another possible source of progenitor cells could be proliferating papillary tubular cells, which exhibited strong PCNA staining at day 4. The decline of PTEC proliferation together with defective differentiation resulted in the development of tubular atrophy. In this model, induction of active caspase-3 in the PTEC from the S3 segment demonstrated the contribution of PTEC apoptosis in tubular atrophy. Till now, only two *in vitro* studies observed such programmed cell death induced by AA exposure.[25,26]

Our data also demonstrated that AA intoxication was associated with defective antioxidative enzyme activation and mitochondrial damage. Transient iNOS overexpression by PTEC could explain elevated urinary excretion of NO*x*.[27]

During the chronic phase, despite an enhanced glutathione peroxidase activity, the decline of antioxidant catalase and Cu/Zn-SOD activities confirmed a decreased capacity to neutralize oxidative bursts. Peroxinitrite production and lipid peroxidation (elevated levels of TBARS) contributed to the chronic interstitial inflammation.[28] Decreased PTEC eosinophilia and diffuse cytoplasmic cytochrome *c* staining were compatible with mitochondrial damage as previously proposed.[29] Chemical anoxia (mitochondrial energy store depletion)[30] could cause PTEC structural injury[31] and dysfunction.[9,10,32,33]

The pathological significance of EMT in renal fibrosis is still controversial.[1,2,34–36] One point of contention is the contribution of EMT to fibroblast formation given the fact that most forms of chronic renal disease are characterized by thickening rather than disruption of the tubular membrane. Given our data, the possible involvement of EMT could be restricted to the basement membrane thickening process rather than an effective source of interstitial fibroblasts. Early migration of dedifferentiated epithelial cells could not be excluded but was unlikely. It was difficult to conclude that interstitial S100A4 + cells originated from EMT. The lack of S100A4 specificity for fibroblasts was already described.[37] On the contrary, the peritubular increase in vimentin-positive

Figure 5 | Time course of NEP immunoperoxidase staining during the chronic phase of AAN; NEP/vimentin and vimentin/Ki-67 double staining in representative control and AA rats. (**a**) Progressive decrease in the percentage of NEP + PTECs in AA rats (gray boxes), as compared to controls (white boxes). Data are median values together with the interquartile ranges and the min–max values; $*P < 0.05$, $**P < 0.01$, $***P < 0.005$ vs controls. (**b**, day 3) Constitutive NEP expression on the brush border of PTECs (S3 segment) (arrow) and vimentin expression by glomerular endothelial cells (star) in a control rat. (**c**) Cytoplasmic staining of vimentin (arrow) in differentiated PTEC (star) after 3 days of AA injections. Progressive accumulation of vimentin-positive PTECs (arrow) exhibiting loss of NEP staining (star) from (**d**) day 7 to (**e**) day 35. (**f**, day 5) Coexpression of Ki-67 and vimentin by PTECs (arrows) in an AA rat. Sections were counterstained (**b–e**) with Mayer's hematoxylin and (**f**) with eosin. Original magnification: × 400.

cells might suggest an activation of resident fibroblasts. As α-SMA + cells accumulated around atrophic tubules in areas of enhanced TGF-β and collagen type I and III expression, the involvement of TGF-β in the local activation of quiescent fibroblasts into myofibroblasts should be considered.[38–41]

To conclude, AA tubulotoxicity resulted in defective activation of antioxidative enzymes and mainly mitochondrial damage. Loss of epithelial markers was concomitant to *de novo* expression of mesenchymal cell markers and disruption of the tubular basement membrane. Despite an early induction of proliferation and dedifferentiation, PTEC did not regain a mature epithelial phenotype. The progressive tubular atrophy was related to a defective regeneration of PTEC and induction of apoptosis secondary to caspase-3 activation. In the absence of transmembrane migration of PTEC displaying the typical signs of EMT, the interstitial accumulation of vimentin-stained cells in areas of TGF-β expression suggested an increase in activated resident

fibroblasts, which are responsible for collagen deposition, indicating their crucial role in the development of interstitial fibrosis.

MATERIALS AND METHODS
Experimental protocols
Experimental procedures performed in 4-week-old male Wistar rats (Elevage Janvier, Le Genest Saint-Isle, France)[42] approved by the local Ethic Committee for Animal Care were conducted according to the National Guidelines for the Care and Use of Laboratory Animals.

In our model of experimental AAN,[8] contrary to previous studies in the cyclosporine model, we showed that TI lesions were independent of salt intake modulation.[42] Therefore, male Wistar rats receiving a normal sodium diet were used for this study.

We performed two successive protocols as follows: the first one ($n = 60$ rats) investigated the period from day 1 to day 5 of AA injections (hereafter referred to as acute phase) and the second one ($n = 60$ rats) investigated the period from day 7 to day 35 (hereafter referred to as chronic phase). Six rats from the AA group and six
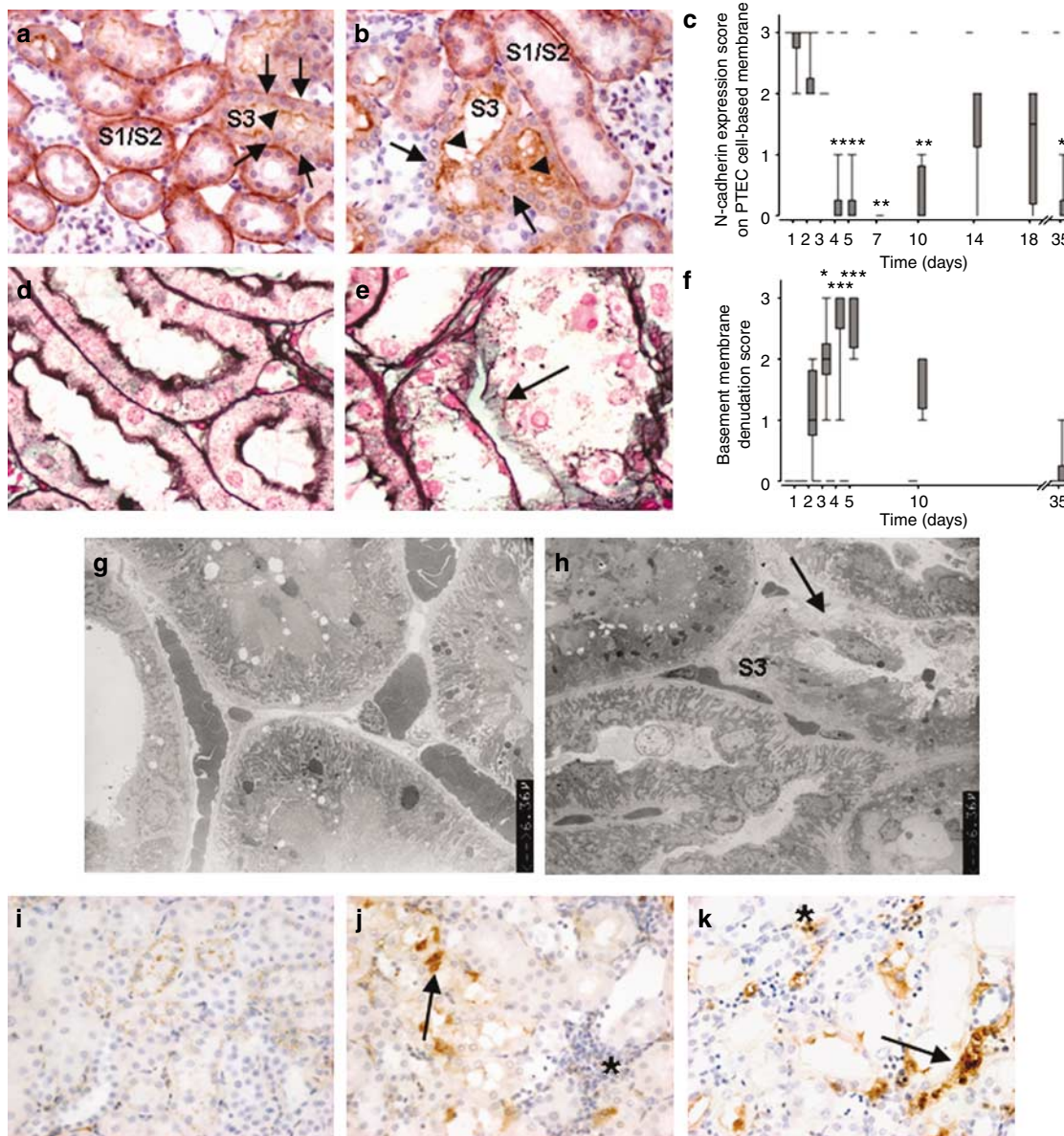
Figure 6 | Representative photomicrographs and time course of the semiquantitative score of N-cadherin and Jones membrane staining. Ultrastructural aspect of the tubular basement membrane of the proximal tubules from the S3 segment. Tissue TGF-β expression in both rat groups. (**a**) In control rats, typical basolateral N-cadherin location (arrows) and NEP + PTEC (S3 segment) (arrowhead). (**b**) Early disappearance of N-cadherin (arrows) at the basolateral membrane of mature PTECs as assessed by the presence of intact nuclei and NEP expression (arrowheads) in rats after 3 days of AA injection. (**c**) Significant and persistent decrease in basal N-cadherin expression by PTECs from S3 segment in AA rats (gray boxes) as compared to controls (horizontal bars). (**d**) Intact tubular and glomerular membranes in a control rat. (**e**, day 2) In an AA rat, detachment of PTECs (arrow) from the basement membrane and marked focal membrane denudation (arrow) limited to the S3 segment. (**f**) Enhanced score of tubular basement membrane denudation in AA rats (gray boxes) as compared to controls (horizontal bars). Data are median values together with the interquartile ranges and the min–max values; *P < 0.05, **P < 0.01, ***P < 0.005 vs day 1. (**g**) Intact morphology of PTEC and the tubular basement membrane in a control rat. (**h**, day 2) Tubular basement membrane rupture (arrow) typically seen in AA rat. (**i**) Constitutive TGF-β expression in a control rat. (**j**, day 3 and **k**, day 35) Enhanced and persistent TGF-β staining in PTECs (arrows) and interstitial accumulation (stars) in AA rats. (**a**, **b**, and **i–k**) Sections were counterstained with Mayer's hematoxylin. Original magnifications: (**a**, **b**, and **i–k**) × 400; (**d** and **e**) × 1000. (**g** and **h**) Sections were counterstained with uranyl acetate and lead citrate. Original magnification: × 1100; kindly provided by C Lebeau, PhD (Laboratoire de Recherche sur le Métabolisme des Peptides, Faculty of Medicine, Université Libre de Bruxelles, Brussels, Belgium).

control rats were killed at the following time points: days 1, 2, 3, 4, 5, 7, 10, 14, 18, and 35 to obtain the kinetics of investigated events.

Weight-matched animals were randomized into two groups: the AA group received AA (10 mg per kg of body weight) and the control group received a solvent of AA (polyethylene glycol 400;

Fluka Chemie, Buchs, Switzerland) in daily subcutaneous injections. After intraperitoneal anesthesia with ketamine HCl (Merial, Brussels, Belgium) and 2% xylazine (Bayer, Brussels, Belgium), a blood specimen was obtained by cardiac puncture. Kidneys were rapidly harvested and processed. One half of the kidney was fixed in
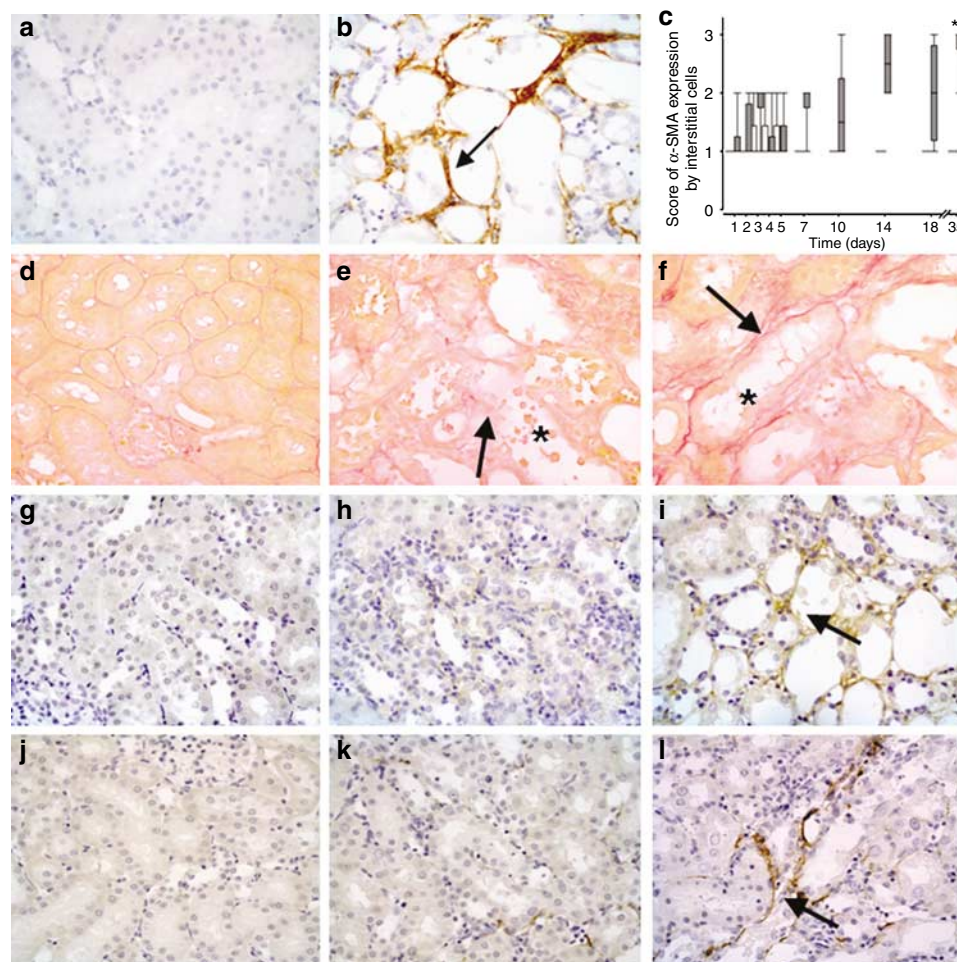
Figure 7 | Kidney α-SMA tissue expression and time course of α-SMA semiquantitative evaluation. Sirius red and collagen type I and III staining in representative control and AA rats. (**a**) Absence of α-SMA expression in controls. (**b** and **c**) Progressive interstitial accumulation of α-SMA-positive cells (arrow) in AA rats (gray boxes) as compared to controls (horizontal bars). Data are median values together with the interquartile ranges and the min–max values; *$P < 0.05$, **$P < 0.01$ vs day 1. (**d**) As compared to controls, (**e**, day 10) remodeling of the basement membrane (arrow) of necrotic tubules (star) and (**f**, day 35) marked thickening of the basement membrane (arrow) of degenerative tubules (star) in AA rats. (**g** and **j**) Absence of collagen type I and III immunostaining in control kidneys. In AA rats, progressive apposition of collagen type I (**h**, day 10 and **i**, day 35) and collagen type III (**k**, day 10 and **l**, day 35) in the external parts of the medullary rays. (**a**, **b**, and **g–l**) Sections were counterstained with Mayer's hematoxylin. (**d–f**) Sirius red staining. Original magnification: ×400.

a buffered solution of 4% formaldehyde (pH 7.4) and paraffin-embedded (formalin-fixed paraffin-embedded) for morphological and immunohistochemical evaluations. The remaining half and samples of contralateral kidney cortex were immediately frozen in liquid nitrogen ($-80\,^\circ$C) for biochemical evaluation. Urine specimens obtained 24 h before killing the animals were stored at $-20\,^\circ$C for further analysis. Variables studied were summarized in Table 1.

Renal histopathology

The TI injury semiquantification was evaluated on hematoxylin/eosin- and Goldner's trichrome-stained formalin-fixed paraffin-embedded sections.[8] Complete kidney sections were analyzed with a light microscope (Carl Zeiss, Oberkochen, Germany) using a ×20 magnification lens by two investigators (AAP and FDD) blind to the group origin of the rats (AA vs control). The scoring systems were defined as follows: *tubular necrosis*: 0, normal tubules; 1, rare single necrotic tubule; 2, several clusters of necrotic tubules; 3, confluence of necrotic clusters; *tubular atrophy*: 0, normal tubules; 1, rare single atrophic tubule; 2, several clusters of atrophic tubules; 3, confluence of

atrophic tubular clusters; *lymphocytic infiltrate*: 0, absent; 1, few scattered cells; 2, group of lymphocytes; 3, widespread infiltrate; *interstitial fibrosis*: 0, absent; 1, minimal fibrosis; 2, moderate fibrosis; 3, severe fibrosis.

Tubular basement membrane staining (2 μm sections) was performed with the Artisan Jones basement membrane stain kit (DakoCytomation, Glostrup, Denmark).

For collagen-specific labeling (4 μm sections), 0.1% Sirius red F3B in saturated picric acid (both from Sigma-Aldrich, Bornem, Belgium) was used.

Electron microscopy was performed as previously reported.[43] Briefly, kidney cortex samples were fixed (4% glutaraldehyde), post-fixed (2% osmium tetroxide), dehydrated, and embedded in Epon. The semithin sections were stained with toluidine blue. Ultrathin sections counterstained with uranyl acetate and lead citrate were examined with a Zeiss EM109 electron microscope (Carl Zeiss).

Biochemical evaluation of renal function

Plasma and urinary Cr excretion levels were determined as previously described.[8]
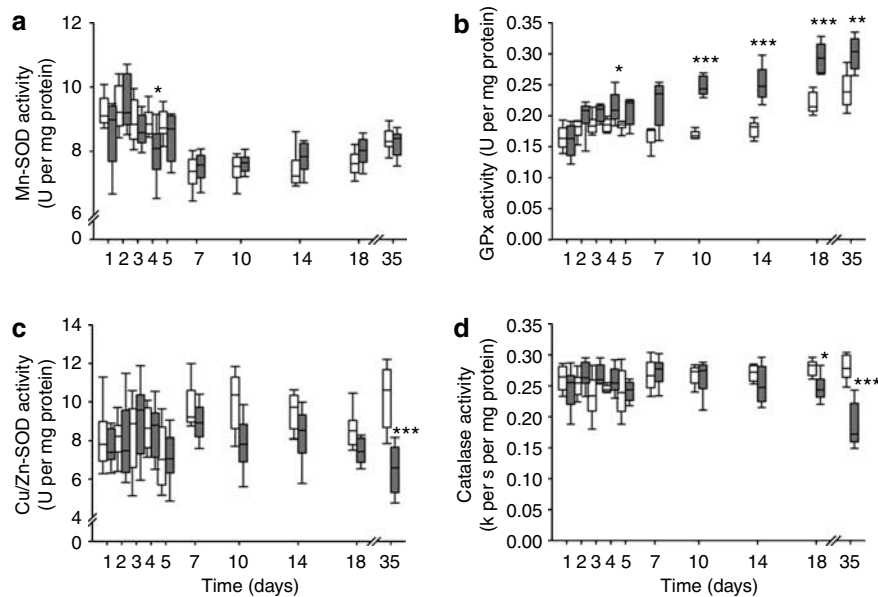
Figure 8 | Time courses of renal cortex antioxidant enzyme activity in control and AA rats. (a–c) In control (white bars) and AA rats (gray bars), renal cortex activity of (**a**) Mn-SOD, (**b**) glutathione peroxidase (GPx), (**c**) Cu/Zn-SOD, and (**d**) catalase was assessed. Data are median values together with the interquartile ranges and the min–max values; $*P < 0.05$, $**P < 0.01$, $***P < 0.005$ vs controls.
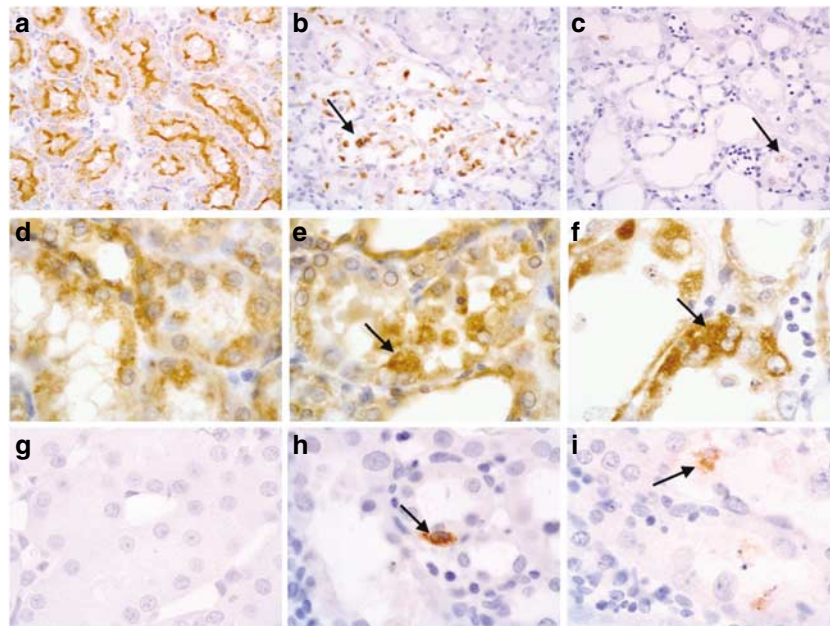
Figure 9 | Representative photomicrographs of iNOS, cytochrome *c*, and cleaved caspase-3 staining in renal medullary rays from control and AA rats. (a) Pattern of iNOS expression in controls. (**b**, day 4 and **c**, day 35) Progressive disappearance of iNOS staining (arrow) from PTEC in AA rats. (**d**) Granular cytoplasmic expression of cytochrome *c* in controls. (**e**, day 4 and **f**, day 35) Diffuse cytoplasmic cytochrome *c* staining in a non-necrotic PTEC (arrow), corresponding to its release from the mitochondrial membrane into the cytoplasm. (**g**, day 3) Absence of caspase-3 immunostaining in a control rat. (**h**, day 10 and **i**, day 35) Cytoplasmic expression of active caspase-3 in tubular cells (arrows) from AA rats, reflecting an induction of tubular cell apoptosis. Sections were counterstained with Mayer's hematoxylin. Original magnifications: (**a–c**) × 200; (**d–i**) × 1000.

Determination of DPPIV urinary activity

Urinary activity of DPPIV was monitored by spectrofluorometric method. Two diluted urine samples were incubated at 37 °C with the synthetic substrate for DPPIV, leucine-7-amido-4-methyl-coumarin (Bachem, Dubendorf, Switzerland). The fluorescence of free AMC was measured at excitation and emission wavelength of 367 and 440 nm, respectively. Results were calculated as mean of fluorescence from two dilutions and expressed as µmol of AMC product per g Cr.

Immunoassay of MCP-1

Urinary excretion of MCP-1 was measured by Rat MCP-1 immunoassay kit, according to the manufacturer's protocol (BioSource International Inc., Nivelles, Belgium) and expressed in ng per g Cr.

Table 1 | Variables studied during the acute and chronic phases of AAN

Variables	Functional significance
Tubulointerstitial injury score, structural and functional renal parameters	
H&E	Evaluation of tubular necrosis and interstitial infiltration
GT	Evaluation of tubular atrophy and interstitial fibrosis
DPPIV	Urinary excretion levels reflect structural integrity of PTEC
Creatinine	Renal function evaluation
Characterization of interstitial inflammation	
CD8	Identification of infiltrating cells expressing CD8 antigen
ED1	Identification of monocytes and tissue macrophages
MCP-1	Secreted by renal residents cells, mononuclear cells, and activated fibroblasts, involved in their recruitment in the zone of tissue injury
DNA damage repair and cells proliferation	
Ki-67	Nuclear protein expressed during all active phases of the cell cycle
PCNA	Cofactor of polymerases involved in DNA synthesis, recombination, and DNA damage repair processes
PTEC dedifferentiation, tubular basement membrane disintegration	
NEP	PTEC brush-border enzyme highly expressed by PTECs from S3 segments
Vimentin	Intermediate filament protein of undifferentiated (mesenchymal) cells, fibroblasts, and endothelial cells
E-cadherin	PTEC apical membrane protein, critical to the cells structure maintenance
N-cadherin	Transmembrane protein mediating intercellular adhesion of PTECs, crucial for maintenance of their polarity
Jones staining	Evaluation of tubular basement membrane integrity
TGF-β	Cytokine involved in fibrosis by stimulating fibroblasts proliferation, EMT process, and collagen deposition
α-SMA	Actin of the smooth muscle cells and myofibroblast cytoskeleton
S100A4	Calcium-binding protein expressed by fibroblasts, T lymphocytes, and plasma cells
Sirius red	Extracellular matrix apposition
Collagen I, III	Evaluation of interstitial fibrosis
Oxidative stress, mitochondrial injury, and apoptosis	
Mn-SOD	Mitochondrial antioxidative enzyme
Cu/Zn-SOD	Extracellular antioxidative enzyme
GPx	Glutathione peroxidase
Catalase	Peroxisomal antioxidative enzyme
TBARS	Products of lipid membrane peroxidation
iNOS	Inducible nitric oxide synthase exacerbating renal oxidative damage[22]
Cytochrome *c*	Marker of structural mitochondrial integrity
Caspase-3	Activated caspase-3 responsible for the induction of cell apoptosis

AAN, aristolochic acid nephropathy; Cu/Zn-SOD, copper/zinc superoxide dismutase; DPPIV, dipeptidyl peptidase IV; EMT, epithelial to mesenchymal transition; GT, Goldner's trichrome; H&E, hematoxylin and eosin; iNOS, inducible nitric oxide synthase; MCP-1, monocyte chemoattractant protein-1; Mn-SOD, manganese superoxide dismutase; NEP, neutral endopeptidase; PCNA, proliferating cell nuclear antigen; PTEC, proximal tubular epithelial cells; α-SMA, α-smooth muscle actin; TBARS, thiobarbituric acid reactive substances; TGF-β, transforming growth factor-β.

Immunohistochemistry

Immunohistochemistry with monoclonal antibodies (Table 2) was performed as detailed previously.[44] Visualization of polyclonal antibodies (Table 2) was obtained using anti-rabbit secondary antibody (DakoCytomation). Control for labeling was carried out with normal serum or antibody diluent (DakoCytomation) instead of primary antibody and showed no staining.

Double immunostaining

First, primary antibody immunoperoxidase staining was performed with diaminobenzidine/substrate (Vector Laboratory, Burlingame, CA, USA). After a microwave elution step, a second complete immunoperoxidase staining was performed with diaminobenzidine/nickel substrate or NovaRed (Vector Laboratory) as a secondary indication system.

Computer-assisted microscopy of tissue area measurement

Quantification of kidney tissue area was adapted from D'Haene *et al.*[45] Per animal, 400 cortical and OSOM fields (17.6 mm^2) on hematoxylin-stained sections were automatically scanned with a ×20 magnification lens of an optical microscope (Olympus, Optical Co. Ltd, Aartselaar, Belgium) and visualized by video camera (Sony Corporation, Tokyo, Japan). The image analysis software measured (mm^2) analyzed tissue area.

Quantification of immunostainings

All quantifying methods were validated by estimation of reproducibility in both rat groups and showed a high rate of concordance (>95%) for intra-assay and inter-assay determinations. Quantifications were performed by one investigator (AP) blind to the group origin of the rats (AA vs control groups). Fields containing more than two glomeruli or large vessels were excluded.

The patterns of Ki-67 and PCNA expression were defined as nuclear staining. Cortical and OSOM areas were analyzed (×40 magnification lens). The PCNA or Ki-67 positively stained PTECs were counted in 30 fields and expressed as an average of PCNA + or Ki-67 + cells per field.

The NEP expression patterns defined as PTEC apical staining and S100A4 cytoplasmic staining were quantified as previously detailed.[9]

The intensity of N-cadherin basolateral membrane staining in PTECs was scored from 0 to 3 (0, absence; 1, very weak; 2, weak; 3, high staining).

The PTEC tubular basement membrane denudation studied on Jones membrane-stained sections and the α-SMA immunostaining were scored from 0 to 3 (0, absence; 1, very rare; 2, rare; 3, frequent). For each rat, a complete kidney section was analyzed with a ×20 and ×40 magnification lenses.

Urinary concentration of NO*x*

Equal amounts of NADH (0.9 mM), FAD (15 μM), and nitrate reductase (0.4 U ml^{-1}) were incubated with diluted urine samples. Equal amounts of lactate dehydrogenase (20 U ml^{-1}), sodium pyruvate (100 mM), and Gries reagent were added. Optical density was measured at 540 nm and expressed in μmol per mmol Cr after comparison to a standard curve.

Cortex antioxidant enzyme activities

Kidney cortex samples were homogenized (2% w/v in 50 mM potassium phosphate with 0.1 mM EDTA and 1% Triton X-100). Catalase activity (×10^3 per s per mg protein) was assayed spectrophotometrically.[46] Total SOD and Mn-SOD activities (after Cu/Zn-SOD inhibition by potassium cyanide) were determined.[47] Cu/Zn-SOD activity (U per mg protein) was calculated as a difference of total SOD and Mn-SOD activity. The glutathione peroxidase activity (selenium + non-selenium-dependent) (U per mg protein) was assayed as detailed.[48]

Table 2 | Primary antibodies and their characteristics

Antibodies	Clone	Dilution	Manufacturers
Avidin–biotin complex visualization system			
Monoclonal mouse IgG anti-human/rat			
CD8a	OX-8	1/300	Serotec, Oxford, UK
CD68	ED1	1/300	Serotec, Oxford, UK
Ki-67	MIB-5	1/100	DakoCytomation, Heverlee, Belgium
PCNA	PC10	1/600	DakoCytomation, Heverlee, Belgium
Cytokeratin 18	Ks18.04	1/50	Chemicon International, Heule, Belgium
NEP	56C6	1/300	Lab Vision, Fremont, CA, USA
Vimentin	V9	1/500	Chemicon International, Heule, Belgium
N-cadherin	6G11	1/100	DakoCytomation, Heverlee, Belgium
α-SMA	1A4	1/1000	DakoCytomation, Heverlee, Belgium
Collagen I	Ab6308	1/300	Abcam, Cambridge, UK
Cytochrome *c*	7H8.2C12	1/100	Lab Vision, Fremont, CA, USA
High-sensitivity two-step visualization system (EnVision system)			
Polyclonal rabbit anti-human/rat			
E-cadherin	H-108	1/1000	Santa Cruz Biotechnology, Santa Cruz, CA, USA
TGF-β	V	1/2000	Santa Cruz Biotechnology, CA, USA
S100A4	A5114	1/2500	DakoCytomation, Heverlee, Belgium
Collagen III	Ab23746	1/500	Abcam, Cambridge, UK
iNOS		1/300	Lab Vision, Fremont, CA, USA
Monoclonal rabbit anti-human/rat			
Cleaved caspase-3	ASP175	1/200	Cell Signaling Technology, Beverly, MA, USA

Ig, immunoglobulin; iNOS, inducible nitric oxide synthase; NEP, neutral endopeptidase; PCNA, proliferating cell nuclear antigen; α-SMA, α-smooth muscle actin; TGF-β, transforming growth factor-β.
The heat-induced antigen retrieval technique was used for all primary antibodies.

Cortex lipid peroxidation

Lipid peroxidation fluorometric assay for measuring TBARS was adapted from Yagi.[49] Briefly, 55 μl of 1% butylated hydroxytoluene in 95% ethanol was added to 4 ml of 40 mmol per l H_2SO_4, followed by 100 μl of cortex homogenate (10% w/v in PBS with 13.4 mM EDTA and 6.5 mM glutathione sulfhydryl), then by 500 μl of 35 mmol per l tungstophosphoric acid and 1 ml of 46 mmol per l thiobarbituric acid in 6 mol per l acetic acid. Samples were heated (95 °C, 1 h). The reaction mixture was extracted with *n*-butanol and measured at 525 nm for excitation and 547 nm for emission using a Hitachi F2000 fluorometer, and TBARS concentration was expressed as pmol per mg protein. Cortical protein (mg) was determined by bicinchoninic acid method (Pierce, Rockford, IL, USA).

Statistical analysis

The TI injury, N-cadherin, PTEC tubular membrane denudation, and α-SMA scores were analyzed in both rat groups by comparing the data from each time point to those of day 1 of the protocol (Kruskal–Wallis analysis of variance and *post hoc* Dunn tests). All the remaining scores obtained from AA and control groups were compared for each corresponding time point (Mann–Whitney *U*-test). Correlations between different variables were determined using the Spearman rank correlation coefficient. A *P*-value lower than 0.05 was considered to be significant.

REFERENCES

1. Liu Y. Renal fibrosis: new insights into the pathogenesis and therapeutics. *Kidney Int* 2006; **69**: 213–217.
2. Forino M, Torredrossa R, Ceol M *et al.* TGF-β1 induces epithelial–mesenchymal transition, but not myofibroblast transdifferentiation of human kidney tubular epithelial cells in primary culture. *Int J Exp Path* 2006; **87**: 197–208.
3. Vanherweghem JL, Depierreux M, Tielemans C *et al.* Rapidly progressive interstitial renal fibrosis in young women: association with slimming regimen including Chinese herbs. *Lancet* 1993; **341**: 387–391.
4. Depierreux M, Van Damme B, Vanden Houte K *et al.* Pathologic aspects of a newly described nephropathy related to the prolonged use of Chinese herbs. *Am J Kidney Dis* 1994; **24**: 172–180.
5. Schmeiser HH, Bieler CA, Weissler M *et al.* Detection of DNA adducts formed by aristolochic acid in renal tissue from patient with Chinese herbs nephropathy. *Cancer Res* 1996; **56**: 2025–2028.

6. Nortier JL, Martinez MC, Schmeiser HH *et al.* Urothelial carcinoma associated with the use of a Chinese herb (*Aristolochia fangchi*). *N Engl J Med* 2000; **342**: 1686–1692.

7. Cosyns JP, Dehoux JP, Guiot Y *et al.* Chronic aristolochic acid toxicity in rabbits: a model of Chinese herbs nephropathy? *Kidney Int* 2001; **59**: 2164–2173.

8. Debelle FD, Nortier JL, De Prez EG *et al.* Aristolochic acids induce chronic renal failure with interstitial fibrosis in salt-depleted rats. *J Am Soc Nephrol* 2002; **13**: 431–436.

9. Lebeau C, Debelle FD, Arlt VM *et al.* Early proximal tubule injury in experimental aristolochic acid nephropathy: functional and histological studies. *Nephrol Dial Transplant* 2005; **20**: 2321–2332.

10. Lebeau C, Arlt VM, Schmeiser HH *et al.* Aristolochic acid impedes endocytosis and induces DNA adducts in proximal tubule cells. *Kidney Int* 2001; **60**: 1332–1342.

11. Bonventre JV. Dedifferentiation and proliferation of surviving epithelial cells in acute renal failure. *J Am Soc Nephrol* 2003; **14**: S55–S61.

12. Lin F, Moran A, Igarashi P. Intrarenal cells, not bone marrow-derived cells, are the major source for regeneration in postischemic kidney. *J Clin Invest* 2005; **115**: 1756–1764.

13. Thomas GL, Yang B, Wagner BE *et al.* Cellular apoptosis and proliferation in experimental renal fibrosis. *Nephrol Dial Transplant* 1998; **13**: 2216–2226.

14. Yang J, Liu Y. Dissection of key events in tubular epithelial to myofibroblast transition and its implications in renal interstitial fibrosis. *Am J Pathol* 2001; **159**: 1465–1475.

15. Anders HJ, Vielhauer V, Schlondorff D. Chemokines and chemokine receptors are involved in the resolution or progression of renal disease. *Kidney Int* 2003; **63**: 401–415.

16. Wilson HM, Walbaum D, Rees AJ. Macrophages and the kidney. *Curr Opin Nephrol Hypertens* 2004; **13**: 285–290.

17. Rabb H. The T cell as a bridge between innate and adaptive immune systems: implications for the kidney. *Kidney Int* 2002; **61**: 1935–1946.

18. Razzaque MS, Taguchi T. Factor that influence and contribute to the regulation of fibrosis. *Contrib Nephrol* 2003; **139**: 1–11.

19. Brezis M, Rosen S. Hypoxia of the renal medulla—its implication for disease. *N Engl J Med* 1995; **332**: 647–655.

20. Bonventre JV, Weinberg JM. Recent advances in the pathophysiology of ischemic acute renal failure. *J Am Soc Nephrol* 2003; **14**: 2199–2210.

21. Maga G, Hubscher U. Proliferating cell nuclear antigen (PCNA): a dancer with many partners. *J Cell Sci* 2003; **116**: 3051–3060.

22. Zhou H, Kato A, Yasuda H *et al.* The induction of cell cycle regulatory and DNA repair proteins in cisplatin-induced acute renal failure. *Tox Applied Pharmacology* 2004; **200**: 111–120.

23. Li Y, Liu Z, Guo X *et al.* Aristolochic acid I-induced DNA damage and cell cycle arrest in renal tubular epithelial cells *in vitro. Arch Toxicol* 2006; **80**: 524–532.

24. Kitamura S, Yamasaki Y, Kinomura M *et al.* Establishment and characterisation of renal progenitor like cells from S3 segment of nephron in rat adult kidney. *FASEB J* 2005; **19**: 1789–1797.

25. Hsin YH, Cheng CH, Tzen JTC *et al.* Effect of aristolochic acid on intracellular calcium concentration and its links with apoptosis in renal tubular cells. *Apoptosis* 2006; **11**: 2167–2177.

26. Balachandran P, Wei F, Lin R-C *et al.* Structure activity relationships of aristolochic acid analogues: toxicity in cultured renal epithelial cells. *Kidney Int* 2005; **67**: 1797–1805.

27. Kone BC, Kuncewicz T, Zhang W *et al.* Protein interactions with nitric oxide synthases: controlling the right time, the right place, and the right amount of nitric oxide. *Am J Physiol Renal Physiol* 2003; **285**: 178–190.

28. Cochrane AL, Ricardo AD. Oxidant stress and regulation of chemokines in the development of renal interstitial fibrosis. *Contrib Nephrol* 2003; **139**: 102–119.

29. Zager RA, Johnson AC, Hanson SY. Proximal tubular cytochrome *c* efflux: determinant, and potential marker, of mitochondrial injury. *Kidney Int* 2004; **65**: 2123–2134.

30. Sinha D, Wang Z, Price VR *et al.* Chemical anoxia of tubular cells induces activation of c-Src and its translocation to the zonula adherens. *Am J Physiol Renal Physiol* 2003; **28**: F488–F497.

31. Lee DBN, Huang E, Ward HJ. Tight junction biology and kidney dysfunction. *Am J Physiol Renal Physiol* 2006; **290**: 20–34.

32. Kabanda A, Jadoul M, Lauwerys R *et al.* Low molecular weight proteinuria in Chinese herbs nephropathy. *Kidney Int* 1995; **48**: 1571–1576.

33. Nortier JL, Deschodt-Lanckman MM, Simon S *et al.* Proximal tubular injury in Chinese herbs nephropathy: monitoring by neutral endopeptidase enzymuria. *Kidney Int* 1997; **51**: 288–293.

34. Strutz F, Zeisberg M. Renal fibroblasts and myofibroblasts in chronic kidney disease. *J Am Soc Nephrol* 2006; **17**: 2992–2998.

35. El Nahas M. Kidney remodelling and scarring: the plasticity of cells. *Nephrol Dial Transplant* 2003; **18**: 1959–1962.

36. Liu Y. Epithelial to mesenchymal transition in renal fibrogenesis: pathologic significance, molecular mechanism, and therapeutic intervention. *J Am Soc Nephrol* 2004; **15**: 1–12.

37. Le Hir M, Hegyi I, Cueni-Loffing D *et al.* Characterization of renal interstitial fibroblast-specific protein 1/S100A4-positive cells in healthy and inflamed rodent kidneys. *Histochem Cell Biol* 2005; **123**: 335–346.

38. Alpers CE, Hudkins KL, Floege J *et al.* Human renal cortical interstitial cells with some features of smooth muscle cells participate in tubulointerstitial and crescentic glomerular injury. *J Am Soc Nephrol* 1994; **5**: 201–209.

39. Chambers RC, Leoni P, Kamiski N *et al.* Global expression profiling of fibroblast responses to transforming growth factor-β1 reveals the induction of differentiation-1 and provides evidence of smooth muscle cell phenotypic switching. *Am J Pathol* 2003; **162**: 533–546.

40. Tamaki K, Okuda S. Role of TGF-beta in the progression of renal fibrosis. *Contrib Nephrol* 2003; **139**: 44–65.

41. Strutz F, Neilson EG. New insights into mechanisms of fibrosis in immune renal injury. *Springer Semin Immunopathol* 2003; **24**: 459–476.

42. Debelle FD, Nortier JL, Husson CP *et al.* The renin–angiotensin system blockade does not prevent renal interstitial fibrosis induced by aristolochic acids. *Kidney Int* 2004; **66**: 1815–1825.

43. Boutajangout A, Authelet M, Blanchard V *et al.* Characterisation of cytoskeletal abnormalities in mice transgenic for wild-type human tau and familial Alzheimer's disease mutants of APP and presenilin-1. *Neurobiol Dis* 2004; **15**: 47–60.

44. Nagy N, Legendre H, Engels O *et al.* Refined prognostic evaluation in colon carcinoma using immuno histochemical galectin fingerprinting. *Cancer* 2003; **97**: 1849–1858.

45. D'Haene N, Maris C, Sandras F *et al.* The differential expression of galectin-1 and galectin-3 in normal lymphoid tissue and non-Hodgkin's and Hodgkin's lymphomas. *Int J Immunopathol Pharmacol* 2005; **18**: 431–443.

46. Bergmeyer HU (ed). *Methods of Enzymatic Analysis*. Verlag Chemie: Weinheim, 1974: 673 pp.

47. Marklund S, Marklund G. Involvement of the superoxide anion radical in the autoxidation of pyrogallol and a convenient assay for superoxide dismutase. *Eur J Biochem* 1974; **47**: 469–474.

48. Flohe L, Gunzler WA. Assays of glutathione peroxidase. *Methods Enzymol* 1984; **105**: 114–121.

49. Yagi K. A simple fluorometric assay for lipoperoxide in blood plasma. *Biochem Med* 1976; **15**: 212–216.